Check for updates

A Review on 3D Architected Pyrolytic Carbon Produced by Additive Micro/Nanomanufacturing

Yolita M. Eggeler,* Ka Chun Chan, Qing Sun, Andrés Díaz Lantada, Dario Mager, Ruth Schwaiger, Peter Gumbsch, Rasmus Schröder, Wolfgang Wenzel, Jan G. Korvink, and Monsur Islam *

Additive micro/nano-manufacturing of polymeric precursors combining with a subsequent pyrolysis step enables the design-controlled fabrication of micro/nano-architected 3D pyrolytic carbon structures with complex architectural details. Pyrolysis results in a significant geometrical shrinkage of the pyrolytic carbon structure, leading to a structural dimension significantly smaller than the resolution limit of the involved additive manufacturing technology. Combining with the material properties of carbon and 3D architectures, architected 3D pyrolytic carbon exhibits exceptional properties, which are significantly superior to that of bulk carbon materials. This article presents a comprehensive review of the manufacturing processes of micro/nano-architected pyrolytic carbon materials, their properties, and corresponding demonstrated applications. Acknowledging the "young" age of the field of micro/nano-architected carbon, this article also addresses the current challenges and paints the future research directions of this field.

1. Introduction

Architected cellular materials are a special class of engineering materials, defined as naturally occurring or artificially designed and topologically arranged structures with counterintuitive properties arising from the structure rather than the constituent material.[1,2] One can find various examples of cellular materials in nature exhibiting unique functionalities, such as lamellar structures in conch shells,[3] hexagonal structures of beehives,[4] and wood.[5] Man-made foams and honeycomb architectures are widely used cellular materials due to easy manufacturability. The recent emergence of additive manufacturing technologies enables the fabrication of architected materials with complex architectures. Advances in micro/nanotechnologies, particularly in laser-based processes, have further facilitated additive manufacturing at the micro and nanoscale.[6,7] Even though the majority of the additive micro/nano-manufacturing processes rely on polymeric materials, architected materials with other materials, including metal,[8,9] semiconductor oxides,[10] and ceramics,[11,12] have already been demonstrated. Advanced and powerful computational methods further facilitate designing intricate architectural features optimized for specific applications.

Y. M. Eggeler, Q. Sun
Microscopy of Nanoscale Structures & Mechanisms (MNM), Laboratory for Electron Microscopy (LEM), Karlsruhe Institute of Technology
Engesserstr. 7, D-76131 Karlsruhe, Germany
E-mail: yolita.eggeler@kit.edu

K. C. Chan, W. Wenzel
Karlsruhe Institute of Technology
Institute of Nanotechnology
Hermann-von-Helmholtz-Platz 1, 76344 Eggenstein-Leopoldshafen,
Germany

A. D. Lantada
Department of Mechanical Engineering
Universidad Politécnica de Madrid
José Gutiérrez Abascal 2, Madrid 28006, Spain

The ORCID identification number(s) for the author(s) of this article can be found under https://doi.org/10.1002/adfm.202302068

D. Mager, J. G. Korvink, M. Islam
Karlsruhe Institute of Technology
Institute of Microstructure Technology
Hermann-von-Helmholtz-Platz 1, 76344 Eggenstein-Leopoldshafen,
Germany
E-mail: monsur.islam@kit.edu

R. Schwaiger
Institute of Energy and Climate Research (IEK)
Microstructure and Properties of Materials (IEK-2)
Forschungszentrum Jülich GmbH, 52425 Jülich, Germany

P. Gumbsch
Institute for Applied Materials
Karlsruhe Institute of Technology
76131 Karlsruhe, Germany

P. Gumbsch
Fraunhofer Institute for Mechanics of Materials IWM
79108 Freiburg, Germany

R. Schröder
Heidelberg University, Centre for Advanced Materials
Im Neuenheimer Feld 225, D-69120 Heidelberg, Germany

**ADVANCED
SCIENCE NEWS**

www.advancedsciencenews.com

**ADVANCED
FUNCTIONAL
MATERIALS**

www.afm-journal.de

Carbon is a fascinating candidate in nature's material library and is often considered "the material for the future" due to its unique mechanical, electrical, thermal, tribological, and biological properties, enabling its use in a diverse range of applications in science and technology.[13,14] The unique electronic structure of carbon allows the formation of robust carbon-carbon covalent bonds in various hybridization states (sp, sp^2, sp^3), enabling the existence of various carbon allotropes in the solid state.[15,16] The last three decades have witnessed a technological revolution in micro/nanodevices using carbon nanotubes (CNTs) and graphene. Even though these devices exhibit exceptional performances, they majorly feature 2D geometries. Higher-order patterning of CNTs and graphene requires mixing these nanomaterials into a polymeric matrix.[17,18] However, such a nanomaterial/polymer composite often compromises the desirable properties of these carbon materials. One effective alternative way of structuring carbon materials is the patterning of an organic polymeric precursor, followed by pyrolysis at a high temperature.[19] The resulting pyrolytic carbon (PyC) contains a mixture of sp^3-hybridized amorphous carbon and sp^2-hybridized graphene layers, and the sp^2/sp^3 ratio varies with the precursor materials and pyrolysis conditions. The often cited properties of PyC include high mechanical strength and stiffness, wide potential stability window, excellent chemical inertness, high biocompatibility, high thermal stability, and tunable electrical and electrochemical properties.[20,21] Initial efforts in micro/nanopatterning of PyC majorly relied on the UV photolithography-based patterning of the precursor material, which is popularly known as carbon micro/nano-electromechanical systems (C-MEMS and C-NEMS).[19,22] However, the C-MEMS/C-NEMS predominantly led to the fabrication of 2D and 2.5D structures. Recent advances in additive manufacturing of polymeric materials have demonstrated fabricating 3D complex architectures with a resolution in the micro- and nanoscale. A subsequent pyrolysis step converts such micro/nano-architected polymeric structures to micro/nano-architected PyC. Notably, a significant geometrical shrinkage occurs during the pyrolytic conversion. The shrinkage further facilitates achieving significantly higher resolution compared to the polymeric additive micro/nanomanufacturing process. Combining the interesting properties of PyC with complex architectures, the design-controlled fabrication of architected PyC has already been demonstrated to exhibit exceptional properties for several applications. Even though the field of architected 3D PyC is relatively new, the exceptional properties of architected PyC have been attracting more and more attention in the scientific community. This article reviews the current literature on 3D architected PyC materials fabricated using different additive micro/nano-manufacturing technologies.
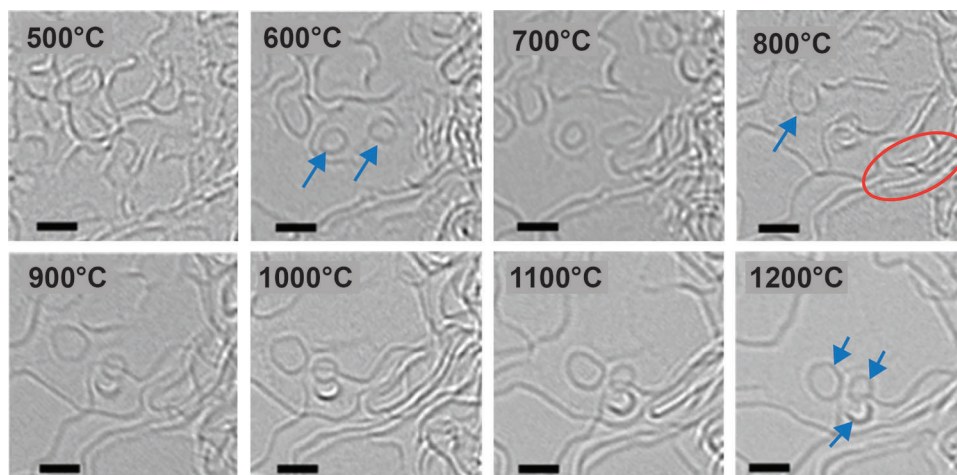
The key factor in fabricating 3D architected PyC is the polymer-to-PyC conversion during pyrolysis. This article presents a brief overview of the pyrolysis mechanism to understand this material conversion. The physicochemical properties of 3D micro/nano-architected PyC are significantly different than that of the bulk PyC materials. The size effect, particularly in nanoarchitected PyC, plays a significant role in this dissimilarity. The resulting physicochemical properties of 3D PyC are further enabled by structural complexity. We discuss the current additive micro/nano-manufacturing for architected PyC and describe the achievable scale and structural complexity. The current applications of 3D PyC materials are next detailed, showcasing their exceptional performances. Finally, current challenges in this "young" field of 3D micro/nano-architected PyC are addressed with the intention of painting the future direction of the field.

2. Pyrolyis and Pyrolytic Carbon

In general terms, pyrolysis refers to the thermochemical decomposition of an organic precursor under the exclusion of oxygen, not limited to only polymers. Pyrolysis of a gaseous hydrocarbon leads to chemical dissociation of the hydrocarbon, followed by deposition of the resulting carbon, which is most popularly known as chemical vapor deposition (CVD).[23,24] Furthermore, pyrolysis is widely used for producing biofuel and biogases from waste polymers.[25,26] However, these processes are not related to the fabrication of architected PyC. This article focuses only on the pyrolysis processes leading to the conversion of a polymer precursor into carbon materials.

The pyrolysis mechanism and the nature of resulting PyC are highly dependent on the chemical composition of the precursor,[28] structural dimensions,[28,29] heating conditions,[30,31] external stresses,[32] and the extent of crosslinking in the case of epoxy resins.[33] Therefore, it is challenging to decipher the pyrolysis mechanism. Over the years, many experimental and theoretical efforts have been made to understand the pyrolysis mechanism for different polymeric precursors. Architected PyC typically uses epoxy resins as precursor polymers. One notable study of gaining an understanding of the pyrolysis mechanism at the molecular scale includes the in situ transmission electron microscopy (TEM) heating investigation of SU-8 epoxy photoresist, an epoxy resin widely used in C-MEMS and C-NEMS technologies for fabricating architected carbon structures, by Sharma et al.[27]. The general scheme of pyrolysis features the following events. In the first stage of pyrolysis, the precursor polymer thermochemically decomposes within a temperature range of 300–500°C, depending on the chemical composition of the polymer, resulting in a significant amount of volatile byproducts, and leaving behind a carbon-rich highly disordered amorphous material. The release of the volatile byproducts yields a significant geometrical shrinkage of the material. Upon further heating, carbon-heteroatom bonds within the carbon-rich material start to cleave, followed by the formation of new carbon-carbon bonds.[34] The pyrolysis-induced evolution of the highly disordered carbon material at the molecular level for temperatures above 500°C was investigated by in situ heating in the TEM, as shown in **Figure 1**. Above 750°C, many of the carbon atoms start rearranging themselves to form networks of graphene fragments (shown in the high-resolution TEM image for 800°C in Figure 1).[27] Along with the graphene fragments, many fullerene-like closed-loop carbon structures also start to form, which tend to migrate within the carbon matrix with increasing temperature, as indicated by the blue arrow shown in Figure 1. The increasing temperature further leads to the reconstruction of the graphene fragments, increasing the graphene crystallite size (L_a) and stack thickness (L_c). At a temperature between 900 and 1200°C, the resulting PyC material contains a significant amount of highly disoriented long-range and short-range graphene layers and a small amount of curved

**ADVANCED
SCIENCE NEWS**

www.advancedsciencenews.com

**ADVANCED
FUNCTIONAL
MATERIALS**

www.afm-journal.de

Figure 1. in situ high resolution TEM pyrolysis investigation of SU-8 photoresist. The approached temperature heating steps are indicated in the upper left corner of each sub-figure and the scale bar corresponds to 1 nm. In the images of 600 and 800°C, the formation of fullerene-like closed-loop graphene layers is indicated by arrows, while the arrows in the image for 1200°C indicate the final positions of these fullerene-like structures. The red ellipse in the TEM image for 800°C indicates the formation of long-range graphene layers. Adapted under the term of CC–BY license .[27] Copyright 2018, the Authors, published by Springer Nature.

fullerene-like carbon structures.[27,35] Such PyC is also referred to as glassy carbon.

Recent advances in computation methods have also enabled studying pyrolysis mechanisms at the atomic level. For example, Reactive Molecular Dynamics simulations have been used by several researchers to gain a deeper understanding of the pyrolysis processes. In the interest of architected PyC, Montgomery–Walsh et al. modeled the pyrolysis of SU-8 for studying the changes on the molecular level at different stages of pyrolysis, namely the temperature ramping stage, the isothermal holding stage, and the ramp time stage.[36] The findings on the molecular transformation at different stages of pyrolysis are summarized in **Figure 2**. They found that during temperature ramping (7 K ps^{-1}) to 3100 K, after the thermochemical breakdown of SU-8, carbon atoms started to rearrange themselves to form complex structures with 5-, 6-, and 7-membered carbon rings. The small graphene flakes with 6-membered carbon rings continued growing larger and longer through ring formation on their edges with further temperature increase. During the isothermal holding stage, long chains of sp-carbons were also formed at the dangling bond of the graphene chains. The isothermal exposure resulted in forming of a complex carbon structure containing flat graphene-like sheets and curved and cage-like carbon structures of sp_2 carbons driven by non-6-membered carbon rings. During the cooling stage, these complex structures continued consolidating into multi-layer and more complex structures with a tubular core and long graphene sheets. In particular, the duration of the isothermal heating had the most significant role in forming the curved and stacked graphene layers. Furthermore, the formation of several functional groups was also observed at the edge of graphene sheets. This study gives an excellent overview of the molecular transformation of the pyrolysis process. However, this study is specific to SU-8 epoxy resins. It is well-established that the chemical composition of the polymer plays the most important role in determining pyrolysis behavior. Molecular dynamic studies of other epoxy resins used in differ-ent 3D micro/nano-manufacturing processes of PyC are yet to be performed.

As mentioned earlier, significant geometrical shrinkage occurs during pyrolysis, which is attributed to the release of volatile gaseous byproducts during the thermochemical decomposition of the precursor material. The shrinkage is highly dependent on the precursor materials,[37] heating conditions,[38] geometry and dimensions of the architectures,[38,39] and their kinematics.[40] For a given precursor and heating condition, the surface area to volume ratio of any architected structure plays the most crucial role in determining the shrinkage,[38,39] as the degassing of the volatile pyrolysis byproducts is expected to occur from the surface of the structure. For architected PyC, a typical shrinkage of individual structural elements ranges from 60% to 85%,[41] whereas a maximum volumetric shrinkage of up to 97% has been reported.[42]

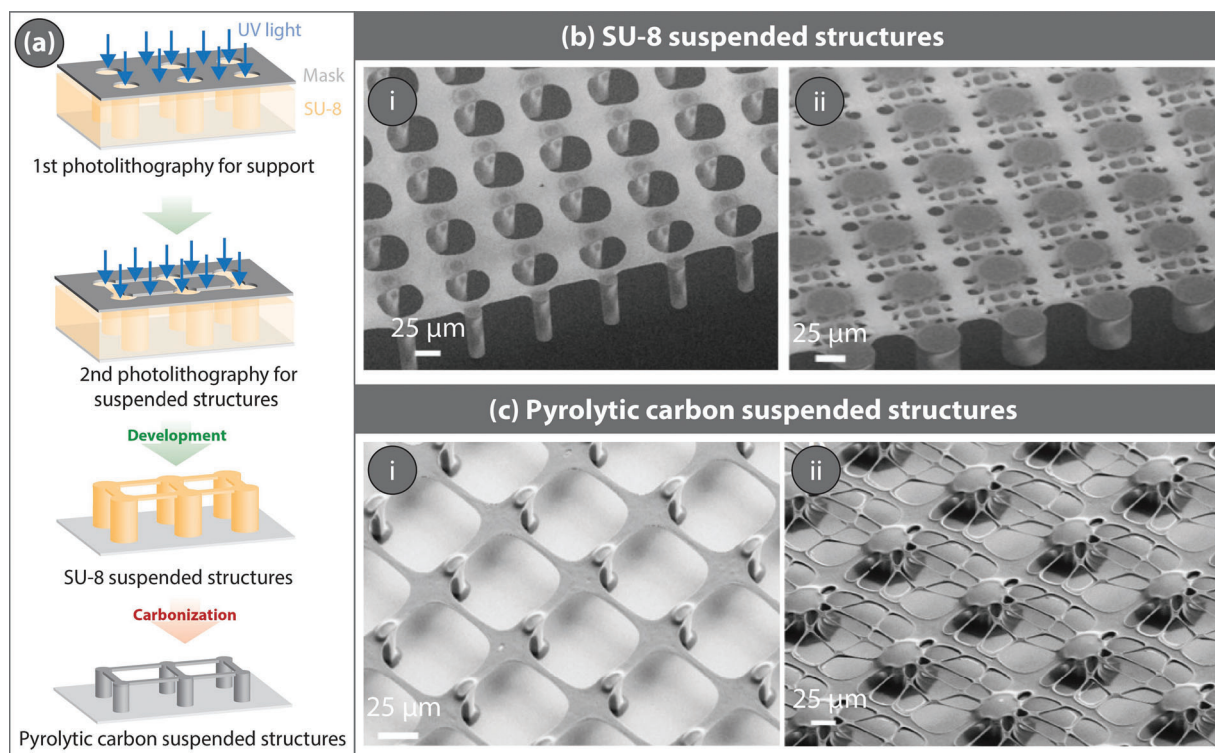## 3. Additive Micro/Nano-Manufacturing Processes for Carbon

3.1. Carbon Microelectromechanical System (C-MEMS)

The classical route for C-MEMS relies on the patterning of an epoxy photoresist using UV photolithography followed by carbonization in an inert atmosphere.[43] Photolithography is the main process in microelectronics and microelectromechanical systems (MEMS) technologies and refers to the patterning of a polymer using light. Therefore, UV light is typically projected through a shadow mask onto an uncured resin layer. The light solidifies the resin where it hits, while the uncured parts can be washed away. This allows easy and highly parallel creation of polymer structures on a substrate; through pyrolysis, these structures become durable carbon. The first demonstration of using photolithography for patterning photoresist-derived carbon was reported in 1983 by Lyons et al. at AT&T Bell Laboratories, where the authors used this process for depositing carbon films as an
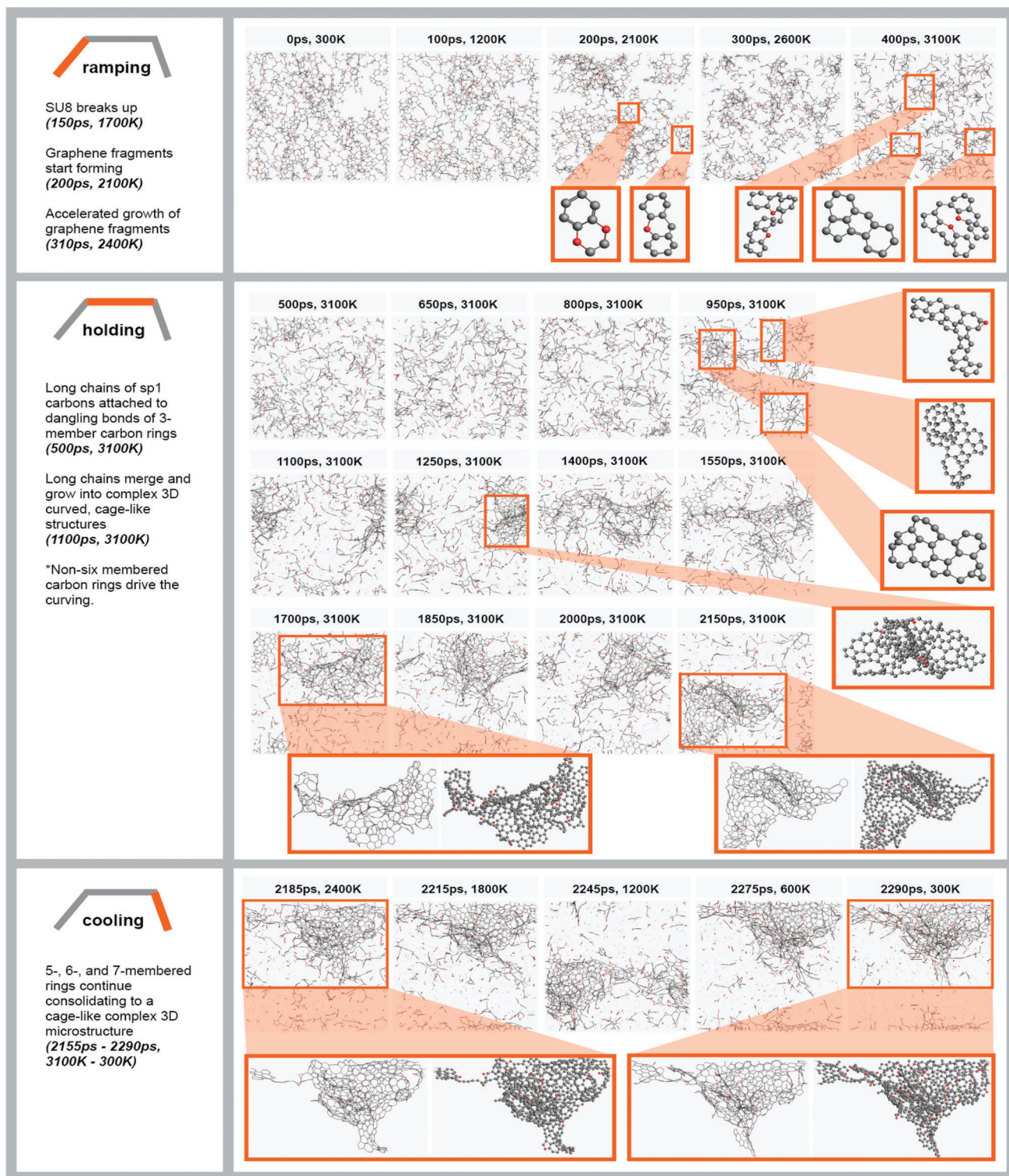
Figure 2. Results from Reactive Molecular Dynamic Simulations of the pyrolysis of SU-8 epoxy resins, showing the molecular transformation at the different stages of pyrolysis. The black spheres represent carbon atoms, whereas the red spheres are oxygen atoms. Note that the temperature employed in this simulation study is much higher than that used in a typical pyrolysis process for PyC (3100 K in simulation vs 900°C in experiments) to accelerate the process in simulations, allowing the reaction energy barriers to overcome easily. Reprinted with permission.[36] Copyright 2021, Elsevier.

**ADVANCED
SCIENCE NEWS**

www.advancedsciencenews.com

**ADVANCED
FUNCTIONAL
MATERIALS**

www.afm-journal.de

Figure 3. a) Schematic illustration of the multistep photolithography process leading to the fabrication of suspended pyrolytic carbon structures. b) Examples of suspended SU-8 structures, and c) their corresponding carbonized structures. Carbonization of (bi,ii) leads to (c,i,ii), respectively. It should be noted how the carbonization-assisted shrinkage led to the stretching of the suspended structures after carbonization. (b,c) are reprinted with permission.[49] Copyright 2016, Institute of Physics.

alternative to chemical vapor deposition.[44] However, it took until the early 2000s that this process started getting more popularity for patterning carbon structures, mainly for 2D patterning. In 2004, Prof. Marc Madou and his team reported the fabrication of high aspect ratio (>10) carbon structures using negative tone photoresists as the carbon precursor.[45,46] They coined the term "C-MEMS", and since then, most of the works involving the structuring of carbon using photolithography and pyrolysis have been identified as C-MEMS.

The most popular photoresist used in C-MEMS is SU-8 due to its low shrinkage, high adhesion to different substrates, ease of curing and processing, and the capability of fabricating high aspect ratio structures.[47] SU-8 is an epoxy-based negative tone photoresist and gets crosslinked when exposed to light, typically with a wavelength of 365 nm. The basic process, based on a single patterning of photoresist, can be considered an additive micromanufacturing route, although the obtained geometries would be normally described as 2.5D. Typical 2.5D structures are arrays of pillars with various cross-sections.[38,43,48] The height of such pillars ranges from a few micrometers to 100 mm. However, multistep photolithography prior to the pyrolysis step leads to even taller carbon pillars.[22]

The multistep photolithography process further facilitates the fabrication of suspended structures, such as bridges, wires, and meshes, over two adjacent supporting pillars.[49–51] A schematic of the process is illustrated in **Figure 3**a, whereas examples of SU-8 and derived PyC suspended structures are shown in Figure 3b,c, respectively. The dimensions of these suspended structures are determined by the capability of the UV-photolithography systems. Madou and colleagues further implemented electrospinning of SU-8 as the tool to fabricate suspended nanofibers with a diameter down to ≈40 nm between two supporting posts fabricated using traditional photolithography.[52,53] It should be noted here that traditional electrospinning in far-field mode was not applicable here, as it does not allow adequate control in positioning and in the number of deposited fibers. Therefore, near-field electrospinning, where the distance between the spinneret and the collector is small (typically <1 cm [54]), was used for the fabrication of the suspended fibers due to its ability to directly write nanofibers. In comparison to the multistep process, Giogli et al. further demonstrated one-step photolithography for fabricating 3D suspended structures.[48] In this study, the authors used longer exposure of the UV light than the optimized exposure duration to initiate the cross-linking of SU-8 on the top layer of the unexposed area adjacent to the exposed area. Such cross-linking led to the formation of suspended structures, including bridges and wires, between two adjacent pillars. The morphology of the suspended structures depended on the shape and size of the cross-section of the pillars, the orientation, and the gap between the pillars. The most crucial challenge in fabricating the suspended carbon structures, regardless of the process, is the shrinkage during pyrolysis. High shrinkage can induce higher residual stress within the structures, resulting in deformation, delamination, and collapse of the structure during pyrolysis. Proper spacing design of the supporting pillars often considerably improves

**ADVANCED
SCIENCE NEWS**

www.advancedsciencenews.com

**ADVANCED
FUNCTIONAL
MATERIALS**

www.afm-journal.de

the quality and reproducibility of the desired suspended carbon structures.[48,50]

3.2. Stereolithography

Stereolithography (SLA) is an additive manufacturing process that facilitates the fabrication of 3D objects of nearly arbitrary shapes using the corresponding 3D model and through layer-by-layer photopolymerization of a photosensitive resin. The process starts with a standard tessellation language (STL) file of the designed 3D object, which is used in most additive manufacturing processes. The STL file is next sliced to convert the 3D model into 2D layers that contain the information of the cross-sections. Layer-by-layer photopolymerization in SLA printing was typically achieved by scanning a laser beam over the liquid resins, followed by pre-programmed vertical movement of the build stage, as originally patented by C.W. Hull.[55] A schematic of an SLA printing system is presented in **Figure 4**a. To enhance the printing efficiency and increase printing speed, projection-based SLA printing has been developed, where digitally masked UV light with cross-sectional details is projected onto the liquid resin for photopolymerization.[56] Digital light processing (DLP)-based SLA printing uses a digital light projector for flashing images of sliced layers to a matrix of digital micromirror devices (DMDs), which selectively redirects the light into the photoresin. To further advance, some DLP printers use a liquid crystal display (LCD) instead of DMD-based light redirection for projecting the light. This shift from a serial Laser-based approach to a parallel UV diode concept dramatically increases the speed while significantly reducing the cost. Details of the different SLA printers have been reviewed elsewhere.[56,57]

In recent years, stereolithography has been getting more and more interest in the research community for facilitating the fabrication of 3D pyrolytic carbon structures with a resolution of around 50 µm. This is particularly due to the availability of low-cost (as low as ≈$100) commercial SLA printers with reasonable resolution and printing quality, the least required infrastructure (particularly for the portable benchtop printers), a straightforward fabrication approach, availability of a wide variety of carbonizable commercial resins, and the possibility to customize the resins. Typically an acrylate-based photoresin is used in SLA printing for carbon structures. Most of the published articles used commercial resins as the starting photoresin,[41,59–62] whereas customized resins, including biopolymer-based resins, have also been demonstrated for SLA-based 3D PyC.[63,64] The precursor material plays the most important role in determining the final shape, size, and macrostructural properties of the final 3D PyC. Since the composition of photoresin in most commercial resins is not accessible to the user, it is difficult to generalize the carbonization process and the resulting properties of 3D PyC based on the precursors. The pyrolysis process also depends on the geometry and the heating protocol used for carbonization. For example, a solid and bulky precursor design often results in a complete collapse of the 3D PyC structure (Figure 4b top row).[30] A bulky structure hinders the complete degassing of the precursor during pyrolysis, as it builds up high pressure due to the trapped gaseous products, which eventually leads to the collapse and fr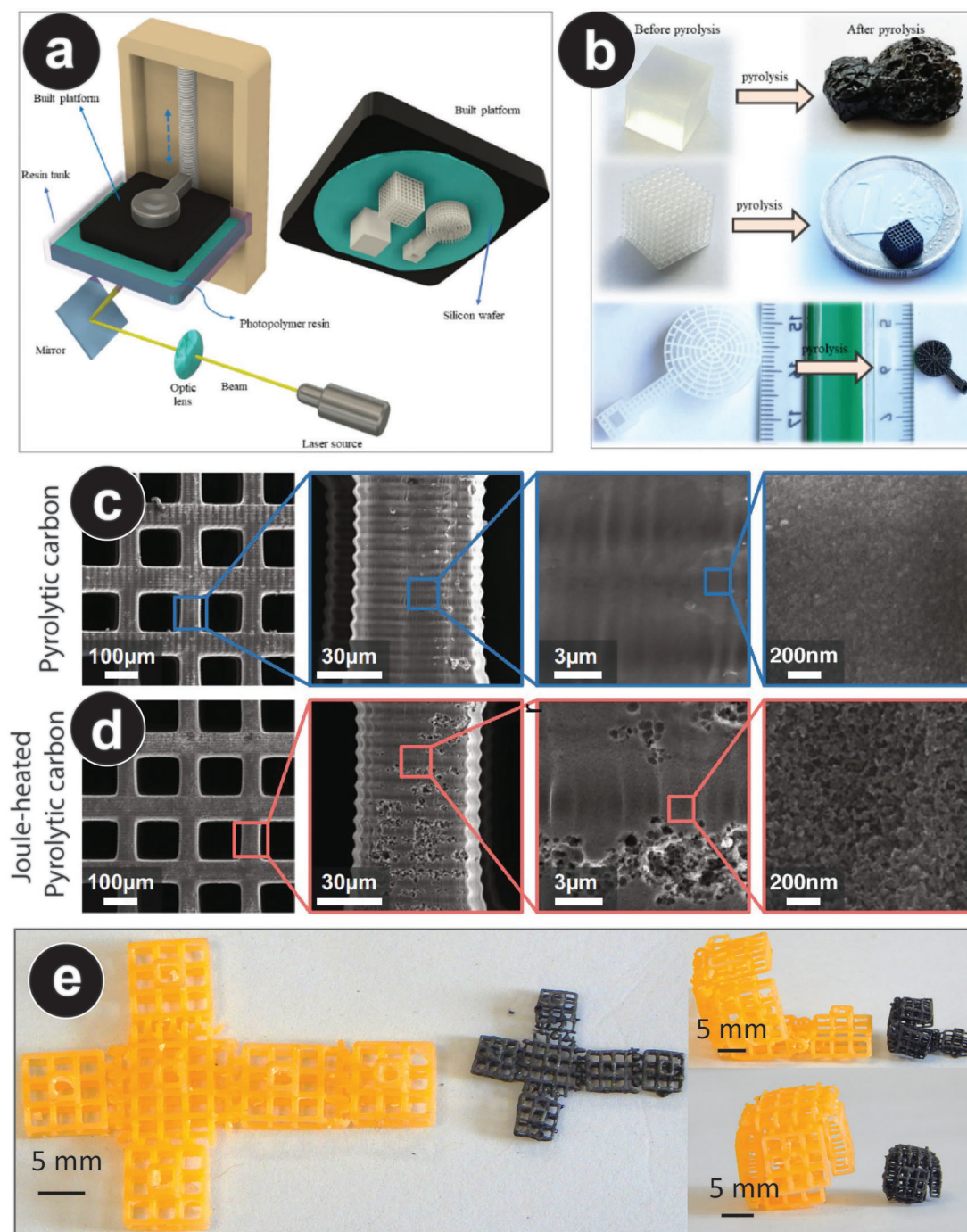acture of the structure. Therefore, designs with lattice elements providing high surface areas for degassing are preferred, as shown in Figure 4b. Even if the lattice elements lead to the retention of the precursor geometry, structural defects can still persist due to incomplete degassing.[41] Typically a heating protocol with ramping up to a final temperature >700°C in an inert atmosphere is used for SLA-based 3D printed PyC. Additional steps in the heating protocol, which include slow heating and prolonged isothermal heating at the decomposition temperature, are useful for complete degassing and thus avoiding bubble formation during the carbonization of the structures.[30,65,66] Such a modified heating protocol also results in higher carbon yield and lower geometrical shrinkage, leading to higher structural density.[30]

SLA-printed PyC majorly features hierarchical porosity with visible surface meso- and macro-pores. The porosity of the 3D PyC can be further enhanced by an additional activation step. For example, Steldinger et al. demonstrated approximately 450% increase in pore volume, resulting in approximately 300% increase in surface area, when activating fabricated 3D PyC at 900°C for 10 h under a CO_2 environment.[67] The enhancement of surface porosity of SLA-printed PyC was further demonstrated by employing a joule-heating to the SLA-printed PyC (Figure 4c,d).[42] The joule-heating converted the surface PyC to nano-graphitic carbon, resulting in the generation of surface pores and a rougher surface. The nano-graphitic coating and higher surface porosity also enhanced the hydrophobicity of the printed structure.

Beyond 3D printing, innovative design for additive manufacturing strategies enables the stereolithographic creation of structures with movable components in connection with the emergent 4D printing field. These kinematic structures, if pyrolyzed under special conditions, can lead to 4D PyC structures with shape-morphing capabilities, which are otherwise extremely challenging to achieve due to the brittle nature of PyC. Our group has recently reported the proof-of-concept structures of 4D PyC to demonstrate the fabrication feasibility, as shown in Figure 4e.[58] However, details of these 4D PyC are yet to be reported.

3.3. Direct Laser Writing or Multi-Photon Polymerization

The pyrolysis–induced shrinkage of polymeric precursors printed using SLA and DLP techniques enables the creation of intricate 3D PyC with fine details as small as approximately 50 µm. Even with cost–effective SLA printers utilizing laser beams with probe diameters of around 150 µm, and DLP systems with pixels of 40 x 40 µm², it is possible to achieve trusses with a width of 250 µm effortlessly. However, to reach architected PyC with even smaller feature sizes, other alternatives are required. Different options enable (sub-)micro(n)-stereolithography, such as scanning using a microscopic objective lens to focus the UV laser beam or the more complex two- and multi-photon polymerization processes, also referred to as direct laser writing (DLW).[68,69] The role of new synthesis photopolymers plays an essential role in achieving the desired precision, together with the hardware and software aspects, as has been studied in detail.[70,71] In short, the simultaneous absorption of two photons was proposed by Maria Göppert–Mayer in 1931,[72] although its experimental demonstration was not achieved until decades later.[73,74] The employment of two–photon polymerization as a lithographic or 3D microstructuring technique

**ADVANCED
SCIENCE NEWS**

www.advancedsciencenews.com

**ADVANCED
FUNCTIONAL
MATERIALS**

www.afm-journal.de

Figure 4. a) Schematic illustration of a typical SLA-based 3D printing system. b) SLA-printed bulk (top row) and architected structures (middle and bottom row) before and after pyrolysis, showing architected structure retaining the precursor geometry, unlike the bulk material. (a,b) are reprinted with permission.[30] Copyright 2020, Elsevier. Surface porosity of SLA-printed c) PyC and d) joule-heated PyC, showing the higher surface porosity of the joule-heated PyC material. Reprinted with permission.[42] Copyright 2020, Springer Nature. e) Sequential configurations of a shape-morphing SLA-printed mechanism before and after carbonization, showing the retention of shape-morphing capabilities of PyC as a feasible approach for fabricating 4D architected PyC. Reprinted with permission.[58] Copyright 2022, Wiley–VCH GmbH.

became possible only with the advent of femtosecond lasers in the 1980s. This breakthrough led to the development of true micro–stereolithography.[75–77] Although the absorption of more than two photons can occur simultaneously, the probability is very low, resulting in a slower fabrication speed. Consequently,

most studies focus on two–photon polymerization and its applications. Multi–photon and two–photon polymerization methods are particularly notable for their ability to cross–link within the focal volume of the laser, enabling genuine three–dimensional writing. This approach avoids the tradi-
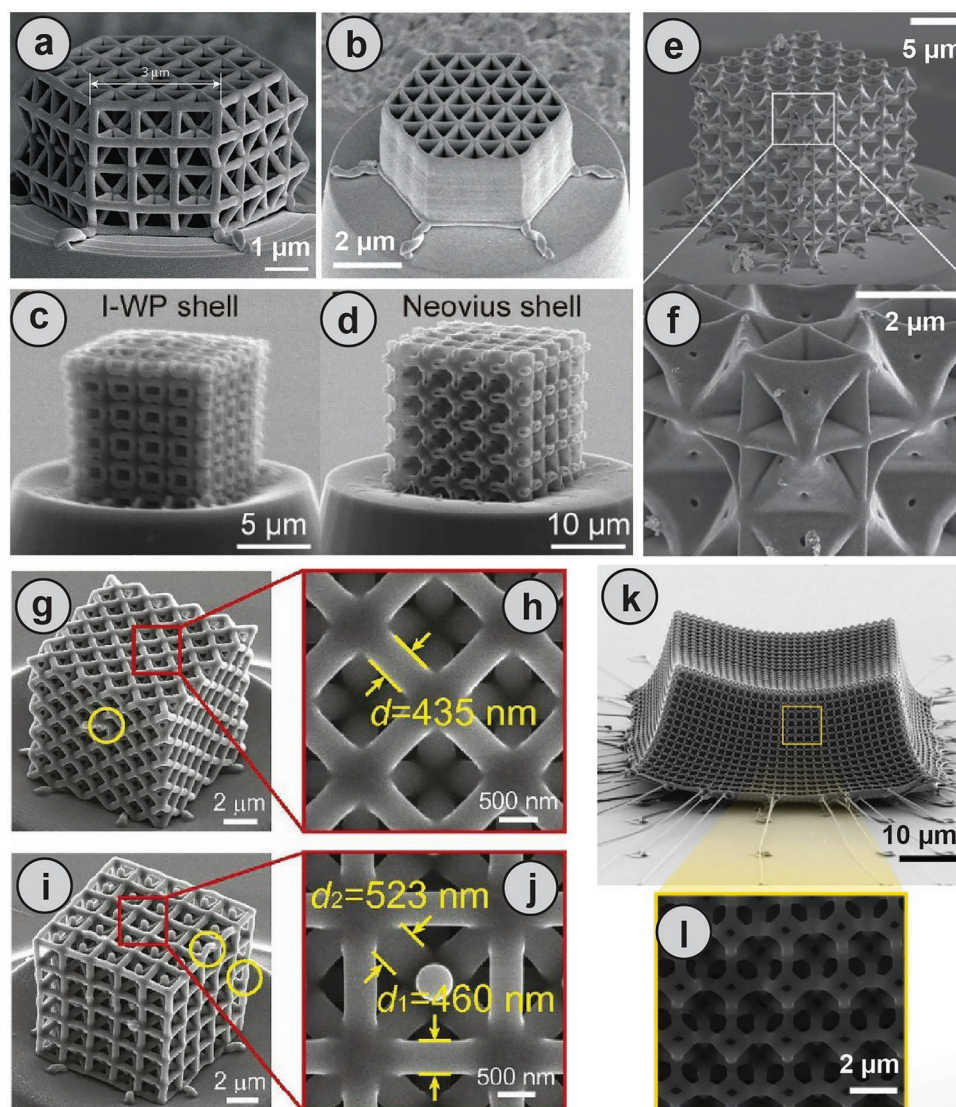
Figure 5. Examples of DLW-fabricated nanoarchitected 3D PyC metamaterials based on different unit cells: a) tetrahedron, b) triangular, c) Schoen's I-graph-wrapped package (I-WP) shell, d) Neovius shell, e,f) cubic+octet plate, g,h) octet truss, i,j) iso-truss, and k,l) tetrakaidecahedron. (a,b) are reprinted with permission.[85] Copyright 2016, Springer Nature. c and d are reprinted with permission.[88] Copyright 2022, National Academy of Sciences. (e,f) are reprinted with permission.[87] Copyright 2020, Springer Nature. (g–j) are reprinted with permission.[86] Copyright 2019, National Academy of Sciences. (k,l) are reprinted with permission.[90] Copyright 2021, Springer Nature.

tional layer–by–layer methods commonly employed in additive manufacturing.[70,71]
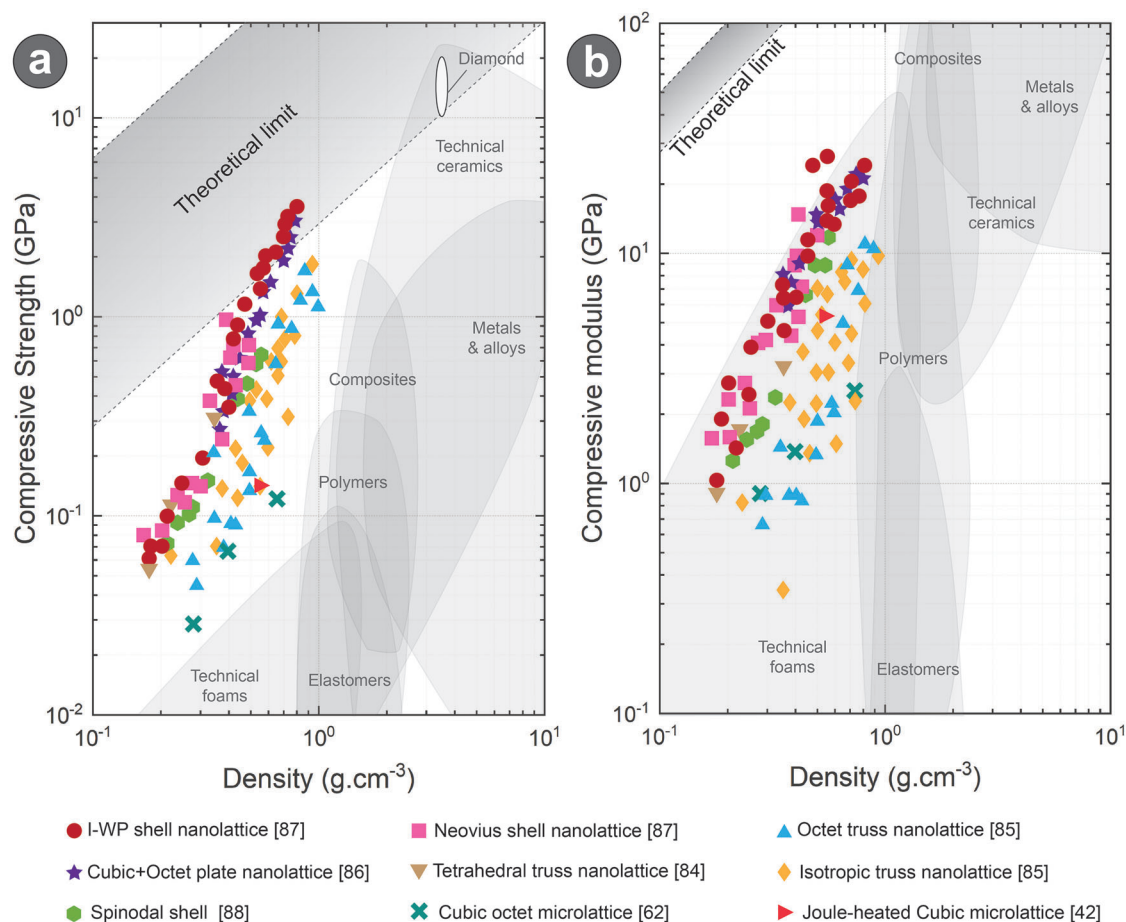
Micro-stereolithography, mainly through two-photon polymerization (2PP), has fostered very relevant discoveries in materials science, especially regarding the emergent field of metamaterials and metasurfaces,[78–80] and constitutes a very successful technology for achieving complex-shaped MEMS/NEMS with innovative features and integrated functionalities,[81,82] as well as for achieving multi-scale micro/nanodevices, by combining it with other lithographic processes or molecular patterning techniques.[83,84] As happens with SLA-based structures, 2PP or DLW objects can be pyrolyzed to achieve PyC with highly precise design-controlled features and to reach submicrometric feature sizes of PyC, leading to nanoarchitected PyC. Examples of several nanoarchitected PyC, particularly mechanical metamaterials with differ-

ent unit cells (discussed in detail in Section 4.1), are presented in **Figure 5**. Among pioneering studies, the combination of 2PP and pyrolysis has led to glassy carbon structures with beam-based nanolattices,[85,86] plate-based nanolattices,[87] shell-based nanolattices,[88,89] and nanowires and nanobridges.[39] Again, the pyrolysis–induced shrinkage in post–2PP printing surpasses resolution constraints, enabling exceptional dimensional details beyond typical technological limits.

4. Applications of 3D Pyrolytic Carbon Structures

4.1. Mechanical Metamaterials

Mechanical metamaterials can be defined as the architected materials with counterintuitive mechanical properties that

**ADVANCED
SCIENCE NEWS**

www.advancedsciencenews.com

**ADVANCED
FUNCTIONAL
MATERIALS**

www.afm-journal.de

Figure 6. Ashby charts of a) compressive strength and b) compressive modulus (stiffness), comparing different micro/nano-architected 3D PyC meta-materials.

originate from the geometry of the structure rather than the properties of the constituting material (for example, negative elastic moduli, negative effective mass densities, and non-linear behaviors).[91] In recent years, architected 3D PyC structures enabled by 3D micro/nano-manufacturing methods have emerged as high-performance mechanical materials. In 2016, in a pioneering work, Bauer et al. reported the fabrication of lightweight PyC nanolattice mechanical metamaterials using two-photon polymerization and subsequent carbonization.[85] They fabricated PyC nanolattice metamaterials with tetrahedral unit cells (Figure 5a) and honeycomb structures with triangular unit cells Figure 5b) with single struts shorter than 1 μm and lattice diameters down to ≈200 nm. The nanohoneycomb structure exhibited a compressive strength up to 1.2 GPa at a structural density of 0.6 g·cm^{-3}, translating to a specific strength of 2 GPa· g^{-1} · cm^3, leaving diamond as the only bulk material with higher specific strength at the time of publication. The compressive strength at fracture was recorded up to 3 GPa, which was analogous to the theoretical strength of bulk glassy carbon. The authors argued that such ultrastrong behavior of the PyC metamaterials was attributed to the scaling effect, topological distribution, and strong constituent PyC material. The topological distribution of the metamaterials helped distribute the applied stress within the structure, which

majorly exhibited bending-dominated failure. On the other hand, the smaller strut dimension restricted the bending failure up to a high limit due to the scaling effect.

The pioneering work by Bauer and colleagues[85] inspired the fabrication of several other lightweight ultra-strong 3D PyC metamaterials with different unit cell designs. Examples of several of such architected PyC with different unit cells are presented in Figure 5c-l. The aim of the majority of these mechanical metamaterials was mainly to push the boundary of specific compressive strength and compressive modulus (also known as stiffness) of architected PyC to reach closer to the theoretical strength of carbon. **Figure 6**a,b presents Ashby diagrams, comparing the compressive strength and stiffness of all the reported 3D PyC mechanical metamaterials, respectively. The upper and lower theoretical limits in the Ashby diagrams correspond to the properties of graphene (the strongest and stiffest known material at the nanoscale) and diamond (the strongest and stiffest known material at the macroscale), respectively. It can be clearly observed that plate (Figure 5e,f) or shell (Figure 5c,d) unit cells favored achieving higher strength and stiffness in contrast to beam truss-based architectures. This is also supported by the topology design principle. In contrast to beam-truss configuration, plate and shell-based structures belong to closed-cell

**ADVANCED
SCIENCE NEWS**

www.advancedsciencenews.com

**ADVANCED
FUNCTIONAL
MATERIALS**

www.afm-journal.de

configurations, which are composed of sheets and thus allow material constrain in two directions, unlike the unidirectional behavior of beams. Upon loading macroscopically, beam-based metamaterials result in different modes of deformation, accommodating large bending strains. In comparison, closed-cell results in tensile membrane stress that efficiently utilizes material volume, independent of the loading direction. Furthermore, closed-cell metamaterials significantly increase the materials interconnectivity within their closed-cell unit cells compared to beam-based unit cells, reducing configurational entropy and increasing the storage of strain energy significantly.[92] The merging of the topological advantages of closed-cell and the excellent material strength and stiffness of micro/nanostructured PyC enabled exceptionally strong and stiff structures at low densities. For example, the cubic+octet plate nanolattice-based metamaterials fabricated by Crook et al.[87] exhibited a compressive strength up to 3 Gpa at a density of 0.792 g· cm^3, translating to a specific strength of $\approx$3.75 GPa· g^{-1} · cm^3. It surpassed the lower limit of the theoretical strength of carbon, thereby surpassing any bulk or architected material. The stiffness of the cubic-octet plate PyC metamaterial was 21.6 GPa, which was also considerably higher than any architected material.[87] Schoen's I-graph-wrapped package (I-WP) shell-based 3D PyC metamaterial fabricated by Wang et al.[88] further exceeded the strength and stiffness of cubic+octet plate nanolattices. The I-WP nanolattices resulted in the highest modulus and strength of 25.68 and 3.52 GPa, respectively, at a density of 0.73 g· cm^{-3}. The authors argued that along with the advantages of closed-cell unit cells, the unique, smooth, and continuous topology of the I-WP shell yielded efficient load distribution within neighboring members without resulting in stress concentrations, leading to an even distribution of strain energy and stress under compressive load. The highest specific strength achieved by these nanolattices was $\approx$4.42 GPa· g^{-1} · cm^3, making them the strongest material reported to date, surpassing all bulk materials (even certain diamond systems) and other architected materials, as also indicated in Figure 6a.
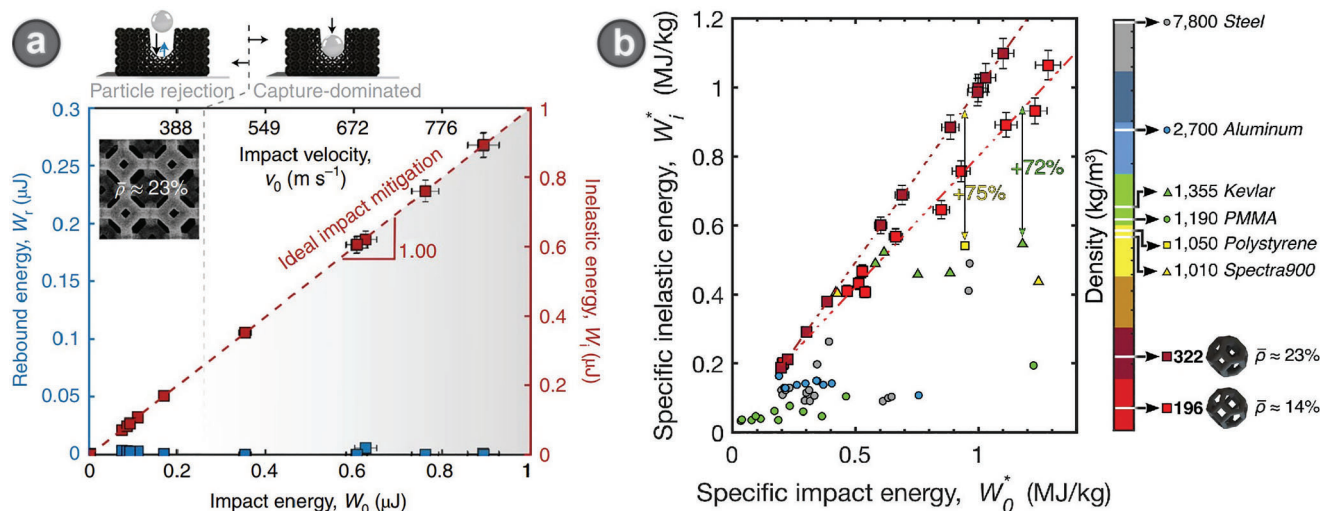
Nanoarchitected 3D PyC indeed enabled a significant enhancement of mechanical properties, as discussed in the previous paragraph. However, these studies only accounted for mechanical performances in quasi-static conditions. In contrast to previous studies, Portela et al. studied the supersonic impact response of nanoarchitected 3D PyC using a tetrakaidecahedron unit cell architecture, featuring beam diameter ranging from 370 to 503nm (Figure 5k,l).[90] The authors chose the tetrakaidecahedron unit cells due to their bending-dominant response, which leads to a non-catastrophic failure, post-yield softening, and constant collapse stress under quasi-static loading, making them beneficial for impact energy absorption. They characterized the extreme dynamic response of the nanoarchitected 3D PyC by accelerating SiO_2 microspheres (diameter=14 μm) using a pulsed laser and making an impact with the metamaterial at a velocity ranging from approximateley 30 m· s^{-1} to 1.2 km· s^{-1}. The nanoarchitected PyC metamaterial with a relative density ($\bar{\rho}$) of 0.37 exhibited complete rebounding of the microsphere without any mechanical failure below an impact velocity of 50 m· s^{-1}, whereas a velocity within 50 to 550 m· s^{-1} resulted in the formation of a crater due to localized brittle fracture, followed by rebounding the microsphere. An impact velocity above 550 m· s^{-1} resulted in fully capturing the microsphere within the crater, without penetrating full sample thickness. The impact resistance energy (or inelastic energy) calculated from the experiments fitted linearly with the impact energy with a slope of 1.0, indicating an ideal energy dissipation response of the nanoarchitected 3D PyC metamaterial, as shown in **Figure 7**a. While comparing with other materials under ballistic impact conditions, the specific impact resistance of the nanoarchitected 3D PyC outperformed all the traditionally used impact-resistant materials, including steel and Kevlar, as shown in Figure 7b.

The current examples of architected 3D PyC metamaterials are majorly populated with nanolattice architectures, utilizing the scaling effect to achieve exceptional mechanical performances. However, 3D PyC metamaterials with microlattice architectures were also studied in a few reports, mainly utilizing the facile and inexpensive fabrication approach of SLA 3D printing. Even though the microarchitected PyC metamaterials could not compete with the mechanical performance of the nanoarchitected metamaterials, they exhibited comparable strength and stiffness for a given density, as shown in Figure 6a,b, respectively.

4.2. Electrodes for Energy Devices

The electrode material in an electrochemical energy device is desired to feature a high active surface area for facilitating electrochemical phenomena and to allow the control of the design and architectural features of the electrode. Activated PyC originating from various organic precursors has been extensively researched as an ideal electrode material candidate due to its high surface area.[93–95] However, in the majority of cases, the activated carbon is used as powder material and a binder is needed to prepare the electrode. The binder often shields the actual surface area of the activated carbon. Furthermore, this process only allows sheet electrodes, which in many cases exhibit sub-optimal shelf-life. Architected 3D PyC is beneficial in these cases, providing strong mechanical resistance while simultaneously facilitating electrochemical reactions essential for energy storage. Further activation of 3D architected PyC can further result in superior performances. For example, in a pioneering work, Wang et al. fabricated a symmetric supercapacitor using SLA-printed 3D architected PyC as binder-free free-form electrodes (**Figure 8**a(i)).[59] They further activated the 3D PyC electrodes through KOH/H_2O activation to enhance the porosity of the electrodes and compared the electrochemical performances with the non-activated 3D PyC electrode and other traditional electrode materials, including carbon paper with and without platinum loading. The activated 3D PyC exhibited a 5.85-fold higher peak current density in the cyclic voltammogram in comparison to the carbon paper compared with carbon papers, as shown in Figure 8a(ii). It is notable that the electrochemical behavior of the 3D architected PyC electrodes also depended on the architectural features. Figure 8a(iii,iv) shows the galvanostatic charge–discharge response and specific capacitance of 3D PyC electrodes with varying distances between adjacent pores. The electrochemical response and the resulting capacitance increased as the designed pore distance decreased. The architected activated PyC resulted in a maximum specific capacitance of around 40 F.g^{-1}. However, the specific capacitance is still lower than other activated carbon-based supercapacitors. Toward enhancing the capacitance of 3D architected

**ADVANCED
SCIENCE NEWS**

www.advancedsciencenews.com

**ADVANCED
FUNCTIONAL
MATERIALS**

www.afm-journal.de

Figure 7. a) Impact energetics for supersonic impact experiments on nanoarchitected 3D PyC metamaterial, featuring a tetrakaidecahedron unit cell shown in Figure 5k,l and $\bar{\rho}$=23%, demonstrating two regimes upon the high-speed impact of a SiO_2 microsphere: formation of crater and rejection of the microsphere, and partial penetration and particle capture. The inelastic energy or the impact resistance energy fits linearly with a slope of 1 with the impact energy, showing excellent energy absorption. b) Comparison of specific inelastic energy (=inelastic energy/mass of the participant material) of nanoarchitected 3D PyC with other traditionally used impact-resistant materials with specific impact energies (=impact energy/mass of the participant material). It shows significant improvement in specific impact resistance in the case of nanoarchitected 3D PyC. Both the figures are reprinted with permission.[90] Copyright 2021, Springer Nature.

PyC, Rezaei et al. decorated the SLA-printed 3D PyC surface with electroactive manganese oxide (MnO_x) nanoparticles.[61] Hybrid architected electrodes were fabricated by wet chemical bath deposition of MnO_2 on SLA-printed 3D resin structures, followed by a calcination/carbonization process, which led to the decoration of highly electroactive crystalline hausmannite-Mn_3O_4 on 3D PyC (Figure 8b(i)). The electrochemical performances of the hybrid electrode were significantly higher than pristine 3D PyC and highly dependent on the loading of MnO_x precursor, as demonstrated by their cyclic voltammograms and electrochemical impedance spectroscopy in Figure 8b(ii,iii), respectively. The hybrid electrode yielded maximum gravimetric and areal capacitances of 186 F·g^{-1} and 968 mF·cm^{-2}, respectively, and retained the capacitance upto >92% even after 5000 cycles.
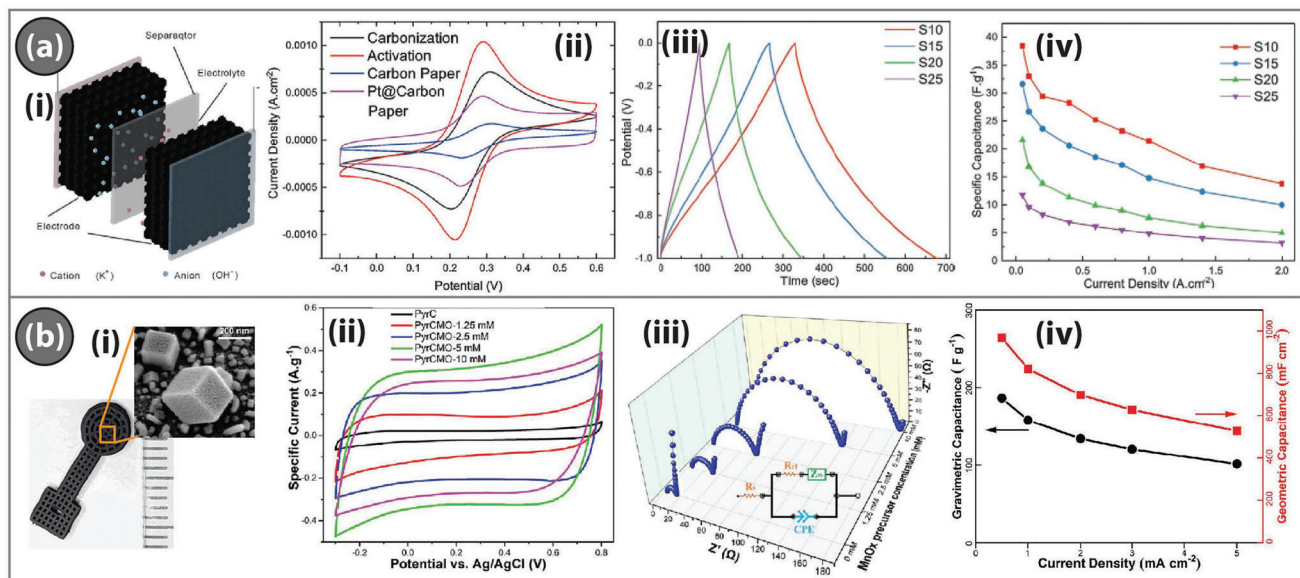
Besides supercapacitor applications, 3D architected PyC has also been demonstrated for battery applications. For example, Narita et al. used 3D architected PyC as a binder-free freestanding electrode in a Li-ion battery.[96] The 3D PyC electrodes exhibited the typical intercalation characteristics of Li-ion battery carbon electrodes, as the galvanostatic cycling at 2 mA g^{-1} displayed a gradual change in voltage above 0.1 V, converging to a plateau at lower voltages, as shown in **Figure 9**a. The electrodes further exhibited a stable long cyclic test at 100 mA g^{-1} by retaining the coulombic efficiency >99.9% for the 2nd through 500th cycle (Figure 9c). However, the capacity decreased rapidly from 131 to 98 mAh g^{-1} by 10 cycles, followed by a gradual decline over 500 cycles. The 3D PyC electrode preserved its architectural features, as shown in Figure 9d, and structural stability after the long cyclic test, which allowed the recycling of the electrode by implementing a simple washing step. In another example, microarchitected activated 3D PyC electrodes were used in a vanadium redox flow battery.[59] The hierarchical porosity of the activated 3D PyC allowed the transport of the VO^{2+}/VO^{2+} species to the mi-

cropores, further facilitating the redox reactions at the micropore surfaces. The superior response was observed for the architectures featuring the minimum thickness and maximum porosity, as these configurations allowed higher superior diffusion.

C-MEMS-driven 2.5D pillar structures have been researched for battery and supercapacitor applications by several researchers.[45,97–100] To date, 3D suspended PyC structures fabricated using C-MEMS have not been investigated for any energy application. However, Mantis et al. characterized the electrochemical behaviors of the 3D suspended PyC and compared them with 2D electrodes.[51] They found that 3D suspended PyC with feature size below 25 μm exhibited three times stronger current response when compared to a corresponding 2D pattern during cyclic voltammetry due to enhanced surface area arising from the suspended 3D configuration. Such a superior current response is suitable for PyC-based high-performance electrochemical energy devices. However, their performance in energy devices still needs to be thoroughly investigated.

4.3. Biomedical Applications

The singular combination of mechanical, electrical, chemical, and biological properties of carbon materials and their adjustability depending on the designed structures, manufacturing route, and processing conditions make C-MEMS and C-NEMS systems suitable for a wide set of biotechnological and biomedical applications, as has been recently reviewed.[47] Here specific biomedical applications of 3D PyC are briefly discussed. Biomedical applications of C-MEMS and C-NEMS involving 3D PyC structures, subsystems, or components, have emerged in parallel to developments in biomedical microfluidics and its application areas and usual configurations, mainly for in vitro applications such

**ADVANCED
SCIENCE NEWS**

www.advancedsciencenews.com

**ADVANCED
FUNCTIONAL
MATERIALS**

www.afm-journal.de

Figure 8. a) Performance of micro-architected activated 3D PyC electrode in supercapacitor: (i) Schematic of the supercapacitor, (ii) Cyclic voltammetry of activated 3D PyC in comparison to other popularly used carbon electrodes, showing a higher current response of the activated architected PyC, (iii) Galvanostatic charge-discharge response and (iv) specific capacitance of the fabricated supercapacitor using activated architected PyC with the varying gap between designed pores (for example, S10 refers to a designed gap of 1.0 mm). Reprinted with permission.[59] Copyright 2020, Wiley–VCH GmbH. b) Supercapacitance performance of Mn_3O_4-decorated micro-architected 3D PyC: (i) A photograph of the architected PyC electrode and an SEM of the Mn_3O_4-particles on the PyC surface, (ii) Cyclic voltammetry and (iii) EIS results of the architected PyC electrodes with varying concentration of surface MnOx particles, and (iv) gravimetric and geometric capacitances of the architected PyC electrode with 5 mM concentration of MnO_x precursor at different current densities in a 1 M H_2SO_4 solution. Reprinted with permission.[61] Copyright 2021, American Chemical Society.

as biosensing platforms,[47] lab-on-a-chip and organ-on-a-chip technologies,[101,102] dielectrophoretic[103,104] and cell-sorting or trapping systems.[105–107] Recently, carbon electrodes for viruses' protein detection against pandemics have been reported.[108]

Regarding biomedical devices for in vivo interactions, carbon micro-/nanoelectrodes and C-MEMS/C-NEMS show potential for human-machine interfaces, including neural probes and health-monitoring implants. Among available examples of contemporary developments, it is important to mention a comprehensive review of carbon-based neural electrodes, dealing with both monitoring and stimulating devices, as well as with 2D and 3D carbon micromanufacturing approaches.[109] In this area, the long-term neural stimulation and low-noise recording of brain activity with highly stable glassy carbon interfaces stand out.[110] PyC micro-needles for drug delivery have also been proposed and demonstrated.[111] Directly connected to in vivo monitoring, glassy carbon electrodes have been developed for minimizing induced voltages, mechanical vibrations, and artifacts in magnetic resonance imaging.[112]

Furthermore, among the most remarkable incipient biomedical applications of architected 3D PyC structures, it is important to highlight their potential as scaffolds for tissue engineering, both for neural[114] and musculoskeletal (**Figure 10**a)[41,63] applications. During cell culture, architected PyC yields better cell adhesion, as the intrinsic surface porosity of PyC provides abundant anchor sites, promoting improved cell proliferation when compared to the cell culture results with the precursor counterpart (Figure 10c). The hierarchical construct of multi-scale 3D PyC further provides favorable microenvironments for cell growth, leading to 3D cell colonization, as shown in Figure 10b,[113] which

can be beneficial for complex articular reconstructions and osteochondral regeneration. Furthermore, PyC materials typically contain only approximateley 1% MRI-sensitive carbon isotope ^{13}C, which makes them almost transparent to the MRI signals and enables the creation of MRI-compatible implants.[114] The feasibility of fabricating architected PyC with ductile nature has also been demonstrated by partial carbonization pathways.[63] The ductility of partially carbonized PyC could be utilized for fabricating biomedical devices, such as coronary stents (Figure 10d).

5. Current Challenges

As discussed in the previous sections, additive micro/nanomanufacturing technologies combined with pyrolysis have enabled the fabrication of micro/nano-architected 3D PyC structures with fascinating geometries and exceptional properties useful for various applications. However, there are also several challenges, solving which may expand the versatility and usability of architected PyC even more. We address some of the current challenges here so that future research can methodically tackle them.

5.1. Understanding the Pyrolysis Process

The most important part of the fabrication process for 3D architected PyC is the carbonization of an architected polymer precursor by pyrolysis. Understanding the carbonization process has been a topic of interest for a long time. Recent technological advances, including molecular dynamic simulation and in situ
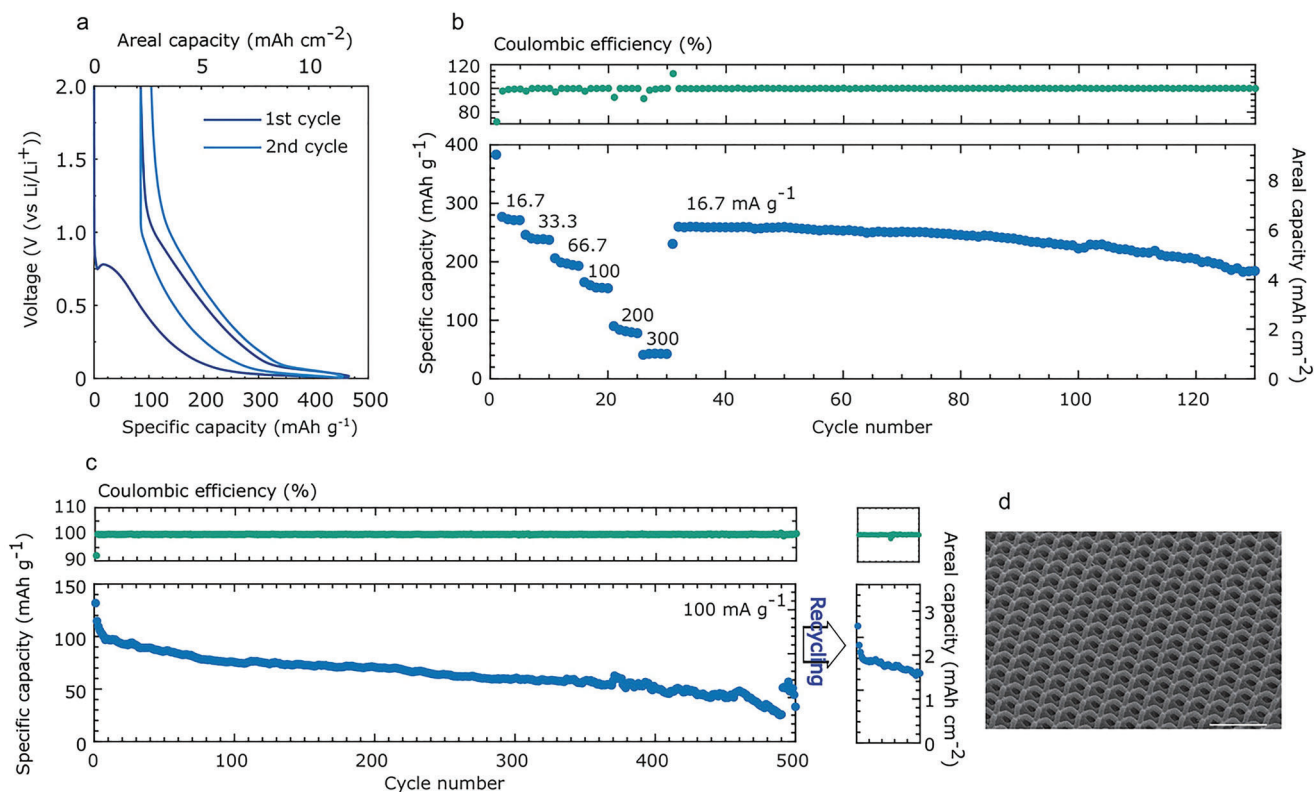
Figure 9. Galvanostatic cycling of microarchitected 3D PyC in a Li-ion battery. a) First two discharge-charge curves at a low current of 2 mA g^{-1}. b) Coulombic efficiency (top) and discharge capacities (bottom) at step currents. c) Specific capacitance and coulombic efficiency for 500 cycles at 100 mA g^{-1}. d) SEM image of a representative microarchitected 3D PyC electrode after >300 cycles at 100 mA g^{-1}. Scale bar is 500 μm for (d). Reprinted with permission.[96] Copyright, 2021 Wiley–VCH GmbH.

heating under electron microscopes, have enabled looking into the process in real-time both at the molecular level and at the morphological and structural level, as discussed in Section 2. However, the majority of the studies are not directed to architected PyC. For example, in situ TEM studies were only performed for organic polymers not related to additive micro/nano-manufacturing. Even though molecular dynamic simulations of the carbonization of SU-8 photoresists are reported, their in situ structural transformation is yet to be studied. Furthermore, the current studies on pyrolysis mechanisms are disjoint from each other, which is even more true in the case of architected PyC. Therefore, the current literature does not allow establishing a correlation among the existing studies to unravel the mechanism for architected PyC. Pyrolysis-assisted shrinkage phenomenon also needs serious consideration. Although a few reports explicitly characterized the shrinkage phenomenon for micro/nano-architected PyC, these studies used simplified geometries, such as cylinders or bars, as the model geometry. It is evident from the existing literature on nano/micro-architected 3D PyC that the volumetric shrinkage is significantly different than that of individual lattice elements and majorly depends on the topological distribution of the constituent lattice elements. There still exists a huge knowledge gap between the shrinkage of individual units and that of the overall 3D architecture. Additionally, the correlations between molecular changes and structural transformations are yet to be investigated. Therefore, comprehensive studies focusing on the transformation from an architected polymer resin to architected PyC correlating the molecular and structural changes with respect to experimental parameters are needed to address these issues to elucidate the pyrolysis process fully. Furthermore, integrating pyrolysis studies of architected PyC with novel methodologies, such as machine learning, can help understand the pyrolytic phenomenon and predict the properties of the resulting architected PyC material.

5.2. Property Driven Precursor Design

Unlike the C-MEMS process, where SU-8 is the standard precursor for PyC, other micro/nano-manufacturing processes, namely SLA and multi-photon polymerization, typically use commercially available resins as the precursor material. The chemical composition of these resins is often unrevealed to the users. It is well known that the carbonization process and resulting PyC properties are highly dependent on the precursor materials. Therefore, the unavailability of information on the chemical composition of the precursor resins makes it complicated to standardize the micro/nano-architected PyC obtained from them. Sometimes changes as simple as the color of the precursor resin could lead to changes in the properties of resulting PyC, restricting their uses in certain applications. Furthermore, the resins are often equipment-specific and do not allow any chemical
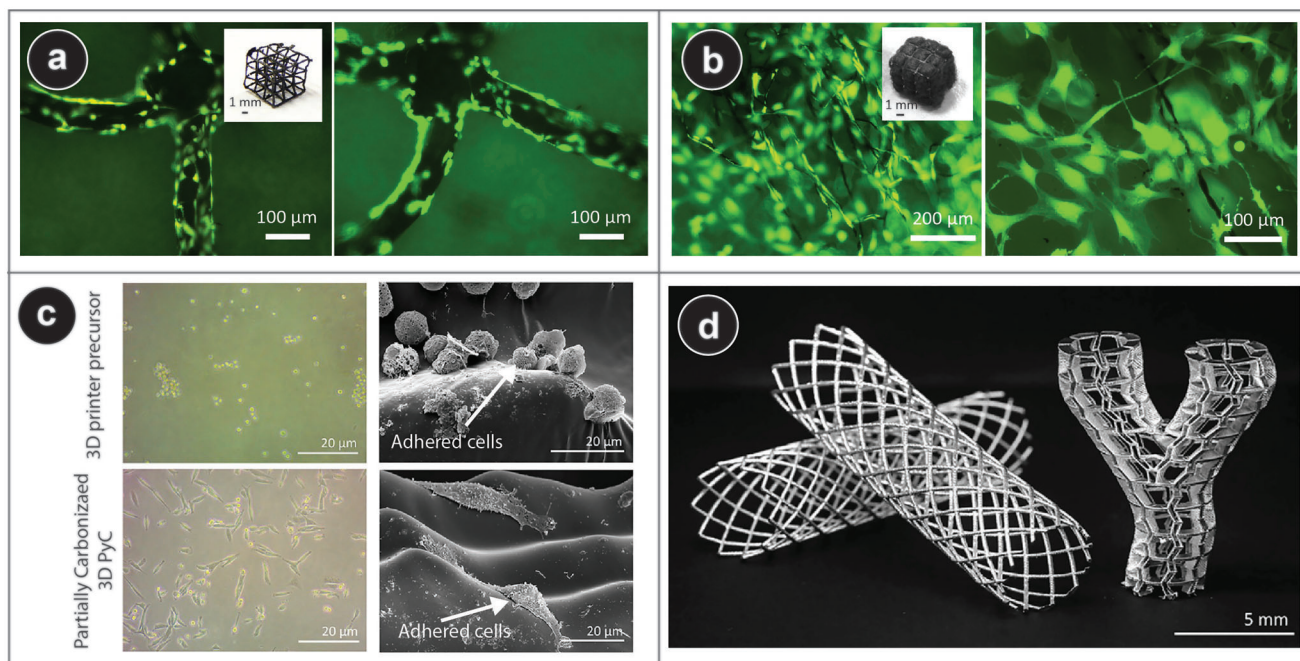
Figure 10. a) Osteoblast-like murine MC3T3-E1 cells cultured on microarchitected 3D PyC on day 3 after cell seeding, showing good cytocompatibility of the architected PyC. Inset shows the microarchitected 3D PyC scaffold used in this study. Adapted with permission.[41] Copyright 2020, Wiley–VCH GmbH. b) The murine MC3T3-E1 cells cultured within a multiscale 3D PyC, obtained by integrating carbon fibers and SLA-printed microarchitected 3D PyC (inset showing the photograph of the multiscale 3D PyC scaffold). Cells proliferated along the PyC microlattices and PyC fibers and also established inter-cellular connections within the microenvironment created by the PyC fibers, leading to a 3D cell colonization. Reprinted with permission.[113] Copyright 2021, Elsevier. c) Cultured cells on an SLA-printed precursor surface and a partially carbonized 3D PyC showing better cell proliferation and enhanced adherence on the PyC surface. d) Examples of coronary stents based on partially carbonized PyC materials utilizing their ductile behavior. (c,d) are reprinted with permission.[63] Copyright 2022, Elsevier.

modifications, which further restrict the customization of PyC properties. Therefore, it is necessary to develop process standardization, where the carbonization and resulting PyC properties can be directly correlated to the precursor resins with known chemical compositions. The capability of precursor customization can lead to pre-designed properties of PyC and even facilitate the fabrication of other carbonaceous materials, including composites and carbides.

5.3. Fabrication of Large-Scale Structures

The applicability of micro/nano-architected PyC has been only demonstrated so far at a lab scale, where a small sample footprint is sufficient for showing the proof-of-concept. However, real-world problems often require a larger material footprint. Therefore, the fabrication of large-scale architected PyC with micro/nano-patterned features is also important. SLA printing, particularly DLP printing, typically allows the fabrication of large-scale architectures due to the availability of large printing areas and fast printing speed. On the contrary, C-MEMS and C-NEMS are predominantly favorable for 2D patterning, even for large areas. As they do not allow much control in the Z-direction, upscaling in the Z-direction is extremely challenging for C-MEMS and C-NEMS. Large-scale structuring is also challenging in multiphoton processes due to their slow printing speed. However, recent progresses in two-photon polymerization have shown the feasi-

bility of fabricating centimeter-scale structures with micrometric feature sizes.[80] The carbonization of these large structures is yet to be reported. Depending on the dimension and structural complexity, the carbonization behavior at the large scale may also be different than the small-scale structures. Particularly, the shrinkage phenomenon of non-isometric structures could be drastic or even catastrophic. Different design adjustments, including additions of supports or microstructural filler designs, might be incorporated to avoid such complications. Therefore, it is important to study the correlation among the carbonization process, micro/nano-structured features, and overall structural volume.

5.4. Sustainability of Pyrolytic Process

With the worldwide concerns over climate change, technological processes must be assessed based on the parameters relating to sustainability throughout the product life cycle. As the field of architected 3D PyC is still in its nascent phase, no study has been dedicated to assessing sustainability issues for PyC. The demonstrated sample volume of micro/nano-architected structures is generally small, which is supposed to have minimal contribution to greenhouse gases. However, the fabrication processes of architected PyC often use highly-complex and powerful infrastructures, including additive micro/nano-manufacturing platforms and high-power furnaces for pyrolysis. Furthermore, many of the precursor materials are synthesized from petroleum

processing, which even asks more for life cycle-oriented carbon footprint analysis. Even though very few studies are available for evaluating the carbon footprint analysis of additive manufacturing processes in general,[115,116] the addressed printing processes haven't been used for PyC materials. Furthermore, the sample volume of architected PyC could significantly increase during its transformation from lab-scale research to large-scale production, which further tends to increase the production carbon footprint. It is, therefore, essential to evaluate the carbon footprint of the fabrication process of architected PyC during its entire life cycle, even at this infant stage of this research field. This will help identify the current challenges in terms of sustainability and find appropriate solutions to them, initiating a future research direction toward "green" fabrication of PyC. To cite an example, more focus could be given to developing bio-based precursors for PyC fabrication, whereas low-temperature pyrolysis of these functional bio-precursors could be studied more intensively to achieve desired properties. Such dedicated studies may also help in sustainable transformation for upscaling the fabrication process.

6. Conclusion and Future Perspective

Additive micro/nano-manufacturing of polymeric precursor combining with a subsequent pyrolysis step enables the fabrication of architected 3D PyC structures with complex architectural details. Pyrolysis-assisted shrinkage further yields a structural dimension significantly smaller than the resolution limit of the involved additive manufacturing technology. The material properties of PyC combined with the 3D architectures enable exceptional properties of the architected PyC compared to bulk PyC material. The size effect, particularly in the case of nano-architected PyC, further enhances the architectural properties. These properties have already enabled architected PyC materials in applications such as structural materials, energy, and health, as reviewed in this article.

Despite impactful demonstrations, it should be noted that the field of micro/nano-architected PyC is still in its infancy, which allows plenty of room for future exploration in terms of fabricating novel architectures and employing them in high-performance applications. There is also a significant scope of improvement within the demonstrated fields of application. For example, the reported energy applications, both supercapacitor and battery, used only micro-architected PyC materials, where the designed pore sizes were still in the micron scale. Nano-architected PyC can lead to PyC electrodes with pore sizes at the nanoscale, which is expected to improve energy storage performances significantly, as smaller pores would result in enhanced surface area, allowing higher active electrochemical sites. Furthermore, judicious designs of nanoarchitecture can facilitate better ion diffusion, improving the performance even more. Furthermore, multiple properties of architected PyC materials could be simultaneously utilized for developing innovative multifunctional materials. For example, architected PyC materials have exhibited exceptional mechanical load-carrying capabilities. Combining such mechanical properties with the electrochemical behavior of PyC could lead to multi-functional sensors, which could sustain a mechanical load and monitor the surrounding environment simultaneously. The multifunctionality of architected PyC can further lead to their use in new application ventures. To give just one exam-

ple, architected PyC could be an important material for space applications. Together with the intrinsic low material density of PyC, the design-based approach of architected PyC makes them highly lightweight, which could potentially replace metals for centimeter-scale components in satellites. Particularly in cube satellites, architected PyC could replace the metallic structures or electronic housing, or even several electronic components utilizing their electrical properties, reducing the overall weight of cube satellites significantly, saving required energy, and prolonging the life of the satellite. The capabilities of such multifunctional properties of architected carbon need to be studied methodically.

Conflict of Interest

The authors declare no conflict of interest.

[1] J. R. Greer, V. S. Deshpande, *MRS Bull.* **2019**, *44*, 750.
[2] Z. Jia, Y. Yu, S. Hou, L. Wang, *J. Mech. Phys. Solids* **2019**, *125*, 178.
[3] D. Hou, G. Zhou, M. Zheng, *Biomaterials* **2004**, *25*, 751.
[4] F. Nazzi, *Sci. Rep.* **2016**, *6*, 1.
[5] M. P. Ansell, in *Wood Composites*, Elsevier, Amsterdam **2015**, pp. 3–26.
[6] Z. Huang, G. Shao, L. Li, *Prog. Mater Sci.* **2022**, *131*, 101020.
[7] M. Vaezi, H. Seitz, S. Yang, *Int. J. Adv. Manuf. Technol.* **2013**, *67*, 1721.
[8] L. Hirt, S. Ihle, Z. Pan, L. Dorwling-Carter, A. Reiser, J. M. Wheeler, R. Spolenak, J. Vörös, T. Zambelli, *Adv. Mater.* **2016**, *28*, 2311.
[9] H. Plank, R. Winkler, C. H. Schwalb, J. Hütner, J. D. Fowlkes, P. D. Rack, I. Utke, M. Huth, *Micromachines* **2019**, *11*, 48.
[10] D. W. Yee, M. L. Lifson, B. W. Edwards, J. R. Greer, *Adv. Mater.* **2019**, *31*, 1901345.
[11] M. Diamantopoulou, T. Tancogne-Dejean, J. M. Wheeler, D. Mohr, *Mater. Des.* **2021**, *208*, 109928.
[12] Z. C. Eckel, C. Zhou, J. H. Martin, A. J. Jacobsen, W. B. Carter, T. A. Schaedler, *Science* **2016**, *351*, 58.
[13] I. A. Edwards, H. Marsh, R. Menendez, in *Introduction to Carbon Science*, Butterworth–Heinemann, Oxford, UK **2013**.
[14] M. J. Madou, V. H. Perez-Gonzalez, B. Pramanick, in *Carbon: The Next Silicon?: Book 2–Applications*, Momentum Press, New York **2016**.

**ADVANCED
SCIENCE NEWS**

www.advancedsciencenews.com

**ADVANCED
FUNCTIONAL
MATERIALS**

www.afm-journal.de

[15] Z. Khalaj, M. Monajjemi, M. V. Diudea, in *Sustainable Nanosystems Development, Properties, and Applications*, IGI Global, Hershey, PA, USA **2017**, pp. 185–213.

[16] V. Georgakilas, J. A. Perman, J. Tucek, R. Zboril, *Chem. Rev.* **2015**, *115*, 4744.

[17] H. Guo, R. Lv, S. Bai, *Nano Mater. Sci.* **2019**, *1*, 101.

[18] S. Agarwala, G. L. Goh, G. D. Goh, V. Dikshit, W. Y. Yeong, in *3D and 4D Printing of Polymer Nanocomposite Materials* **2020**, pp. 297–324.

[19] M. J. Madou, V. H. Perez-Gonzalez, B. Pramanick, in *Carbon: The Next Silicon?: Book 1-Fundamentals*, Momentum Press, New York **2016**.

[20] R. Martinez-Duarte, P. Renaud, M. J. Madou, *Electrophoresis* **2011**, *32*, 2385.

[21] K. Jurkiewicz, M. Pawlyta, D. Zygadło, D. Chrobak, S. Duber, R. Wrzalik, A. Ratuszna, A. Burian, *Iran. J. Mater. Sci.* **2018**, *53*, 3509.

[22] C. Wang, M. Madou, *Biosens. Bioelectronics* **2005**, *20*, 2181.

[23] N. Mishra, G. Das, A. Ansaldo, A. Genovese, M. Malerba, M. Povia, D. Ricci, E. Di Fabrizio, E. Di Zitti, M. Sharon, M. Sharon, *J. Anal. Appl. Pyrolysis* **2012**, *94*, 91.

[24] Y. Zhang, L. Zhang, C. Zhou, *Acc. Chem. Res.* **2013**, *46*, 2329.

[25] M. Sekar, T. Mathimani, A. Alagumalai, N. T. L. Chi, P. A. Duc, S. K. Bhatia, K. Brindhadevi, A. Pugazhendhi, *Fuel* **2021**, *283*, 119190.

[26] G. Su, H. C. Ong, M. Mofijur, T. I. Mahlia, Y. S. Ok, *J. Hazard. Mater.* **2022**, *424*, 127396.

[27] S. Sharma, C. Shyam Kumar, J. G. Korvink, C. Kübel, *Sci. Rep.* **2018**, *8*, 1.

[28] R. Lehrle, *J. Anal. Appl. Pyrolysis* **1987**, *11*, 55.

[29] H. Maleki, L. Holland, G. Jenkins, R. Zimmerman, *Carbon* **1997**, *35*, 227.

[30] B. Rezaei, J. Y. Pan, C. Gundlach, S. S. Keller, *Mater. Des.* **2020**, *193*, 108834.

[31] K. Mondal, G. Pawar, M. McMurtrey, A. Sharma, *Mater. Today Chem.* **2020**, *16*, 100269.

[32] M. Ghazinejad, S. Holmberg, O. Pilloni, L. Oropeza-Ramos, M. Madou, *Sci. Rep.* **2017**, *7*, 1.

[33] E. Fitzer, W. Schäfer, *Carbon* **1970**, *8*, 353.

[34] S. Sharma, A. M. Rostas, L. Bordonali, N. MacKinnon, S. Weber, J. G. Korvink, *J. Appl. Phys.* **2016**, *120*, 235107.

[35] S. Sharma, S. Zorzi, V. Cristiglio, R. Schweins, C. Mondelli, *Carbon* **2022**, *189*, 362.

[36] R. Montgomery-Walsh, S. Nimbalkar, J. Bunnell, S. L. Galindo, S. Kassegne, *Carbon* **2021**, *184*, 627.

[37] M. Islam, P. G. Weidler, D. Mager, J. G. Korvink, R. Martinez-Duarte, *Micromachines* **2022**, *13*, 503.

[38] R. Natu, M. Islam, J. Gilmore, R. Martinez-Duarte, *J. Anal. Appl. Pyrolysis* **2018**, *131*, 17.

[39] B. Cardenas-Benitez, C. Eschenbaum, D. Mager, J. G. Korvink, M. J. Madou, U. Lemmer, I. D. Leon, S. O. Martinez-Chapa, *Microsyst. Nanoeng.* **2019**, *5*, 1.

[40] M. Islam, J. Flach, R. Martinez-Duarte, *Carbon* **2018**, *133*, 140.

[41] M. Islam, A. D. Lantada, M. R. Gómez, D. Mager, J. G. Korvink, *Adv. Eng. Mater.* **2020**, *22*, 2000083.

[42] A. Kudo, F. Bosi, *Commun. Mater.* **2020**, *1*, 1.

[43] R. Martinez-Duarte, M. Islam, R. Natu, *Carbon MEMS*, Springer, Dordrecht, The Netherlands, ISBN 978-94-007-6178-0, **2014**, pp. 1–8.

[44] A. Lyons, C. Wilkins, M. Robbins, *Thin Solid Films* **1983**, *103*, 333.

[45] C. Wang, L. Taherabadi, G. Jia, M. Madou, Y. Yeh, B. Dunn, *Electrochem.* **2004**, *7*, A435.

[46] C. Wang, G. Jia, L. H. Taherabadi, M. J. Madou, *J. Microelectromech. Syst.* **2005**, *14*, 348.

[47] S. Forouzanfar, N. Pala, M. Madou, C. Wang, *Biosens. Bioelectron.* **2021**, *180*, 113119.

[48] E. Giogli, M. Islam, R. Martinez-Duarte, *ECS Trans.* **2016**, *72*, 125.

[49] S. Hemanth, C. Caviglia, L. Amato, T. A. Anhøj, A. Heiskanen, J. Emnéus, S. S. Keller, *Ecs Trans.* **2016**, *72*, 117.

[50] S. Hemanth, T. A. Anhøj, C. Caviglia, S. S. Keller, *Microelectron. Eng.* **2017**, *176*, 40.

[51] I. Mantis, S. Hemanth, C. Caviglia, A. Heiskanen, S. S. Keller, *Carbon* **2021**, *179*, 579.

[52] G. Canton, T. Do, L. Kulinsky, M. Madou, *Carbon* **2014**, *71*, 338.

[53] D. George, A. Garcia, Q. Pham, M. R. Perez, J. Deng, M. T. Nguyen, T. Zhou, S. O. Martinez-Chapa, Y. Won, C. Liu, R. C. Lo, R. Ragan, M. Madou, *Microsyst. Nanoeng.* **2020**, *6*, 1.

[54] A. Sadaf, M. Elter, D. Mager, U. H. Bunz, M. Islam, J. G. Korvink, *Adv. Eng. Mater.* **2022**, 2101740.

[55] C. W. Hull, Apparatus for Production of Three-Dimensional Objects by Stereolithography, **1986**, US Patent 4,575,330.

[56] J. Huang, Q. Qin, J. Wang, *Processes* **2020**, *8*, 1138.

[57] R. Palucci Rosa, G. Rosace, *Macromol. Mater. Eng.* **2021**, *306*, 2100345.

[58] M. Islam, A. D. Lantada, D. Mager, J. G. Korvink, *Adv. Healthcare Mater.* **2022**, *11*, 2101834.

[59] P. Wang, H. Zhang, H. Wang, D. Li, J. Xuan, L. Zhang, *Adv. Mater. Technol.* **2020**, *5*, 1901030.

[60] Y. Katsuyama, A. Kudo, H. Kobayashi, J. Han, M. Chen, I. Honma, R. B. Kaner, *Small* **2022**, *18*, 2202277.

[61] B. Rezaei, T. W. Hansen, S. S. Keller, *ACS Appl. Nano Mater.* **2021**, *5*, 1808.

[62] A. Kudo, D. Misseroni, Y. Wei, F. Bosi, *Front. Mater.* **2019**, *6*, 169.

[63] J. U. Surjadi, Y. Zhou, S. Huang, L. Wang, M. Li, S. Fan, X. Li, J. Zhou, R. H. Lam, Z. Wang, Y. Lu, *Matter* **2022**, *5*, 4029.

[64] P. Blyweert, V. Nicolas, J. Macutkevic, V. Fierro, A. Celzard, *ACS Sustainable Chem Eng.* **2022**, *10*, 7702.

[65] J. Y. Pan, B. Rezaei, T. A. Anhøj, N. B. Larsen, S. S. Keller, *Micro Nano Eng.* **2022**, *15*, 100124.

[66] P. Blyweert, V. Nicolas, V. Fierro, A. Celzard, *Molecules* **2022**, *27*, 2091.

[67] H. Steldinger, A. Esposito, K. Brunnengräber, J. Gläsel, B. J. Etzold, *Adv. Sci.* **2019**, *6*, 1901340.

[68] S. You, K. Miller, S. Chen, *Biofabrication and 3D Tissue Modeling* **2019**, pp. 1–21.

[69] A. Bertsch, P. Renaud, in *Three-Dimensional Microfabrication Using Two-Photon Polymerization*, Elsevier, Amsterdam **2020**, pp. 25–56.

[70] J. Stampfl, R. Liska, A. Ovsianikov, in *Multiphoton Lithography: Techniques, Materials, and Applications*, John Wiley & Sons, Hoboken, NJ, USA **2016**.

[71] S. C. Ligon, R. Liska, J. Stampfl, M. Gurr, R. Mülhaupt, *Chem. Rev.* **2017**, *117*, 10212.

[72] M. Göppert-Mayer, *Ann. Phys.* **1931**, *401*, 273.

[73] Y.-H. Pao, P. Rentzepis, *J. Chem. Phys.* **1965**, *43*, 1281.

[74] P. Franken, A. E. Hill, C. e. Peters, G. Weinreich, *Phys. Rev. Lett.* **1961**, *7*, 118.

[75] E.-S. Wu, J. H. Strickler, W. R. Harrell, W. W. Webb, in *Optical/Laser Microlithography V*, vol. *1674*, SPIE, France **1992**, pp. 776–782.

[76] S. Maruo, O. Nakamura, S. Kawata, *Opt. Lett.* **1997**, *22*, 132.

[77] A. Otuka, J. Almeida, V. Tribuzi, M. R. Cardoso, A. C. Hernandes, D. Correa, C. R. Mendonça, *Mater. Res.* **2014**, *17*, 352.

[78] M. Kadic, G. W. Milton, M. van Hecke, M. Wegener, *Nat. Rev. Phys.* **2019**, *1*, 198.

[79] G. Zyla, A. Kovalev, C. Esen, A. Ostendorf, S. Gorb, *J. Opt. Microsys.* **2022**, *2*, 3031203.

[80] V. Hahn, P. Kiefer, T. Frenzel, J. Qu, E. Blasco, C. Barner-Kowollik, M. Wegener, *Adv. Funct. Mater.* **2020**, *30*, 1907795.

[81] A. J. Otuka, N. B. Tomazio, K. T. Paula, C. R. Mendonça, *Polymers* **2021**, *13*, 1994.

[82] M. Emons, K. Obata, T. Binhammer, A. Ovsianikov, B. N. Chichkov, U. Morgner, *Opt. Mater. Express* **2012**, *2*, 942.

[83] S. Hengsbach, A. D. Lantada, *Biomed. Microdevices* **2014**, *16*, 617.

[84] A. Diaz Lantada, R. Kumar, M. Guttmann, M. Wissmann, M. Schneider, M. Worgull, S. Hengsbach, F. Rupp, K. Bade, M. Hirtz, S. Sekula-Neuner, *Polymers* **2020**, *12*, 655.

[85] J. Bauer, A. Schroer, R. Schwaiger, O. Kraft, *Nat. Mater.* **2016**, *15*, 438.

[86] X. Zhang, A. Vyatskikh, H. Gao, J. R. Greer, X. Li, *PNAS* **2019**, *116*, 6665.

[87] C. Crook, J. Bauer, A. Guell Izard, C. Santos de Oliveira, J. Martins de Souza e Silva, J. B. Berger, L. Valdevit, *Nat. Commun.* **2020**, *11*, 1.

[88] Y. Wang, X. Zhang, Z. Li, H. Gao, X. Li, *Proc. Natl. Acad. Sci.* **2022**, *119*, e2119536119.

[89] A. Guell Izard, J. Bauer, C. Crook, V. Turlo, L. Valdevit, *Small* **2019**, *15*, 1903834.

[90] C. M. Portela, B. W. Edwards, D. Veysset, Y. Sun, K. A. Nelson, D. M. Kochmann, J. R. Greer, *Nat. Mater.* **2021**, *20*, 1491.

[91] X. Li, H. Gao, *Nat. Mater.* **2016**, *15*, 373.

[92] J. Berger, H. Wadley, R. McMeeking, *Nature* **2017**, *543*, 533.

[93] S. Sundriyal, V. Shrivastav, H. D. Pham, S. Mishra, A. Deep, D. P. Dubal, *Resour. Conserv. Recycl.* **2021**, *169*, 105548.

[94] M. Sevilla, R. Mokaya, *Energy Environ. Sci.* **2014**, *7*, 1250.

[95] J. Wang, X. Zhang, Z. Li, Y. Ma, L. Ma, *J. Power Sources* **2020**, *451*, 227794.

[96] K. Narita, M. A. Citrin, H. Yang, X. Xia, J. R. Greer, *Adv. Energy Mater.* **2021**, *11*, 2002637.

[97] G. T. Teixidor, R. B. Zaouk, B. Y. Park, M. J. Madou, *J. Power Sources* **2008**, *183*, 730.

[98] E. Adelowo, A. R. Baboukani, O. Okpowe, I. Khakpour, M. Safa, C. Chen, C. Wang, *J. Power Sources* **2020**, *455*, 227987.

[99] S. Mamidi, A. D. Pathak, A. Gangadharan, C. S. Sharma, *J. Power Sources* **2020**, *473*, 228600.

[100] S. Mamidi, M. Kakunuri, C. S. Sharma, *ECS Trans.* **2018**, *85*, 21.

[101] D. Ha, J. Hong, H. Shin, T. Kim, *Lab Chip* **2016**, *16*, 4296.

[102] R. Martinez-Duarte, R. A. Gorkin III, K. Abi-Samra, M. J. Madou, *Lab Chip* **2010**, *10*, 1030.

[103] R. Natu, M. Islam, D. Keck, R. Martinez-Duarte, *Lab Chip* **2019**, *19*, 2512.

[104] R. Martinez-Duarte, D. Mager, J. G. Korvink, M. Islam, *Front. Med. Technol.* **2022**, 49.

[105] P. Puri, V. Kumar, S. Belgamwar, N. Sharma, *Biomed. Microdevices* **2018**, *20*, 1.

[106] M. Elitas, Y. Yildizhan, M. Islam, R. Martinez-Duarte, D. Ozkazanc, *Electrophoresis* **2019**, *40*, 315.

[107] R. Natu, M. Islam, R. Martinez-Duarte, *Anal. Chem.* **2019**, *91*, 4357.

[108] B. Pramanick, N. Mandal, R. Mitra, *Res. Squ.* **2022**, https://doi.org/10.21203/rs.3.rs-1983819/v1.

[109] M. Devi, M. Vomero, E. Fuhrer, E. Castagnola, C. Gueli, S. Nimbalkar, M. Hirabayashi, S. Kassegne, T. Stieglitz, S. Sharma, *J. Neural Eng.* **2021**, *18*, 041007.

[110] M. Vomero, E. Castagnola, F. Ciarpella, E. Maggiolini, N. Goshi, E. Zucchini, S. Carli, L. Fadiga, S. Kassegne, D. Ricci, *Sci. Rep.* **2017**, *7*, 1.

[111] R. Mishra, B. Pramanick, T. K. Maiti, T. K. Bhattacharyya, *Microsyst. Nanoeng.* **2018**, *4*, 1.

[112] S. Nimbalkar, E. Fuhrer, P. Silva, T. Nguyen, M. Sereno, S. Kassegne, J. Korvink, *Microsyst. Nanoeng.* **2019**, *5*, 1.

[113] M. Islam, A. Sadaf, M. R. Gómez, D. Mager, J. G. Korvink, A. D. Lantada, *Mater. Sci. Eng. C* **2021**, *126*, 112140.

[114] E. Fuhrer, A. Bäcker, S. Kraft, F. J. Gruhl, M. Kirsch, N. MacKinnon, J. G. Korvink, S. Sharma, *Adv. Healthcare Mater.* **2018**, *7*, 1700915.

[115] D. Wang, T. Zhang, X. Guo, D. Ling, L. Hu, G. Jiang, *J. Environ. Sci.* **2022**, *130*, 85.

[116] S. S. Muthu, S. M. Mahesh, *Handbook of Sustainability in Additive Manufacturing*, Vol. 2, Springer, Singapore **2016**, pp. 101–114.

Yolita M. Eggeler received her Ph.D. in Material Science and Engineering in 2018 from Friedrich-Alexander University (FAU) in Erlangen, Germany. Her thesis work focused on investigating nanoscale diffusion and thermomechanical deformation mechanisms in single-crystal superalloys. As an Alexander von Humboldt fellow, she then worked as a postdoc in the Materials Department of the University of California Santa Barbara (UCSB), USA, where she employed advanced electron microscopy to contribute to study couplings between internal strain and magnetism in Heuslers and deformation mechanisms of novel high entropy alloys. In 2020, Eggeler accepted a tenure-track assistant professorship for electron microscopy at the Laboratory for Electron Microscopy (LEM) within the Karlsruhe Institute of Technology (KIT), Germany. In her own research group, Nanoscale Structures & Mechanisms (MNM), she tackles cutting edge material topics, with an emphasis placed on developing new methods and workflows to explore micro- and nanoscale structural evolution in structural and functional materials.

Monsur Islam is a scientist at the Institute of Microstructure Technology at Karlsruhe Institute of Technology (KIT), Germany. He received his Ph.D. in Mechanical Engineering in 2018 from Clemson University, USA. The research activities during his Ph.D. included microfabrication of carbon microelectrodes for healthcare diagnostics and advanced manufacturing of 3D porous carbonaceous materials. The department and the University recognized his research activities by awarding him the prestigious Hitachi High Technologies Electron Microscopy Fellowship, Doctoral Scholastic Award, and Eastman Chemical Award. In 2023, Monsur received the prestigious Marie Sklodowska-Curie Postdoctoral Fellowship for carrying out his research activities at IMDEA Materials Institute in Madrid, Spain. Monsur's current research interests include fabricating carbon-based materials, both 3D structures and flexible devices, for biomedical applications, including tissue engineering scaffolds, flexible electrodes for bio-electronics and biosensors, and microelectrodes for point-of-care diagnosis.